Am J Physiol Regul Integr Comp Physiol 311: R325–R336, 2016.
First published May 25, 2016; doi:10.1152/ajpregu.00463.2015.

Seasonal changes in brown adipose tissue mitochondria in a mammalian hibernator: from gene expression to function

Mallory A. Ballinger, Clair Hess, Max W. Napolitano, James A. Bjork, and Matthew T. Andrews

Department of Biology, University of Minnesota Duluth, Duluth, Minnesota

Submitted 4 November 2015; accepted in final form 24 May 2016

Ballinger MA, Hess C, Napolitano MW, Bjork JA, Andrews MT. Seasonal changes in brown adipose tissue mitochondria in a mammalian hibernator: from gene expression to function. *Am J Physiol Regul Integr Comp Physiol* 311: R325–R336, 2016. First published May 25, 2016; doi:10.1152/ajpregu.00463.2015.—Brown adipose tissue (BAT) is a thermogenic organ that is vital for hibernation in mammals. Throughout the hibernation season, BAT mitochondrial uncoupling protein 1 (UCP1) enables rapid rewarming from hypothermic torpor to periodic interbout arousals (IBAs), as energy is dissipated as heat. However, BAT's unique ability to rewarm the body via nonshivering thermogenesis is not necessary outside the hibernation season, suggesting a potential seasonal change in the regulation of BAT function. Here, we examined the BAT mitochondrial proteome and mitochondrial bioenergetics in the thirteen-lined ground squirrel (*Ictidomys tridecemlineatus*) across four time points: spring, fall, torpor, and IBA. Relative mitochondrial content of BAT was estimated by measuring BAT pad mass, UCP1 protein content, and mitochondrial DNA (mtDNA) copy number. BAT mtDNA content was significantly lower in spring compared with torpor and IBA ($P < 0.05$). UCP1 mRNA and protein levels were highest during torpor and IBA. Respiration rates of isolated BAT mitochondria were interrogated at each complex of the electron transport chain. Respiration at complex II was significantly higher in torpor and IBA compared with spring ($P < 0.05$), suggesting an enhancement in mitochondrial respiratory capacity during hibernation. Additionally, proteomic iTRAQ labeling identified 778 BAT mitochondrial proteins. Proteins required for mitochondrial lipid translocation and β-oxidation were upregulated during torpor and IBA and downregulated in spring. These data imply that BAT bioenergetics and mitochondrial content are not static across the year, despite the year-round presence of UCP1.

brown adipose tissue; mitochondria; hibernation; UCP1; proteomics

THE THIRTEEN-LINED GROUND squirrel (*Ictidomys tridecemlineatus*) is a small, obligate hibernator that transitions readily between homeothermy and heterothermy throughout its circannual cycle. During hibernation, ground squirrels reduce their metabolic rate and use fat stored in white adipose tissue as their primary fuel source (2). This stored lipid is consumed at high rates by brown adipose tissue (BAT), which has evolved to burn fat as a means to rapidly generate heat (reviewed in Ref. 7). Energy is dissipated as heat because the electron transport chain (ETC) is uncoupled from ATP formation by uncoupling protein 1 (UCP1; reviewed in Ref. 7). Heat generation plays a vital role in the endogenous rewarming of ground squirrels via nonshivering thermogenesis during arousal from torpor (reviewed in Ref. 7). In fact, the highest rate of BAT activity occurs during these periodic arousals, referred to as interbout arousals (IBAs), where the animal's body temperature increases 20°C in less than 1 h and is able to return to normothermia within 3 h, as warm blood circulates (Refs. 25, 51; Fig. 1).

The interplay between mitochondria and thermogenesis in BAT is supported by a significant increase in UCP1 transcripts in torpor and IBA compared to spring (23), further validating the importance of BAT's thermogenic role during hibernation. However, the thermogenic capacity and activity of BAT are probably not necessary during spring or summer (i.e., homeothermy); therefore, we hypothesize that BAT mitochondrial function changes seasonally. During hibernation, metabolism in most other tissues can be reduced to conserve energy, but maintenance of BAT function is critical for heat generation needed during arousals. Most mitochondrial metabolic studies in hibernators have been conducted in the liver, which shows metabolic suppression during hibernation (reviewed in Ref. 56). But unlike the liver, BAT contributes significantly to whole organism rewarming during arousal from torpor.

Many aspects of BAT thermogenesis during arousal have been investigated (reviewed in Ref. 7), yet there has been little investigation of mitochondrial metabolism in BAT throughout the circannual cycle of a natural hibernator (reviewed in Refs. 55 and 56). Previous studies on hibernator BAT lack a thorough investigation of mitochondrial bioenergetics between homoeothermic and heterothermic periods (6, 11, 12, 27, 28, 38, 40, 43). Thus, the overall goal of this study is to interrogate BAT mitochondria across the circannual cycle using integrated approaches from gene expression to function. The recently generated thirteen-lined ground squirrel BAT transcriptome (23) has provided inferences on molecular mechanisms of BAT mitochondria. However, mRNA levels do not always correlate with protein abundance and function in living systems (17, 21, 45, 47, 55, 54, 60). Therefore, we estimated changes in mitochondria protein by generating a seasonal BAT mitoproteome in parallel with measurements of functional mitochondrial bioenergetics. Combined with the BAT transcriptome (23) from various seasonal points across the year, this study provides insight into organelle biology (36) and the functional adaptations of BAT mitochondria in a mammalian hibernator.

METHODS

Animal Care and Tissue Collection

All animal care and procedures were approved by the University of Minnesota Institutional Animal Care and Committee (protocol no. 1103A97712). Wild-caught thirteen-lined ground squirrels (*Ictidomys tridecemlineatus*) were captured in central Minnesota and were housed individually upon arrival in the American Association for Accreditation of Laboratory Animal Care-accredited Animal Care Facility located in the University of Minnesota Duluth School of Medicine. All animals were housed at room temperature in a 12:12-h light-dark cycle, and were fed standard rodent chow (Purina, no.

Address for reprint requests and other correspondence: M. T. Andrews; Dept. of Biology, 1035 Kirby Dr., Univ. of Minnesota Duluth, Duluth, MN 55812 (e-mail: mandrews@d.umn.edu).

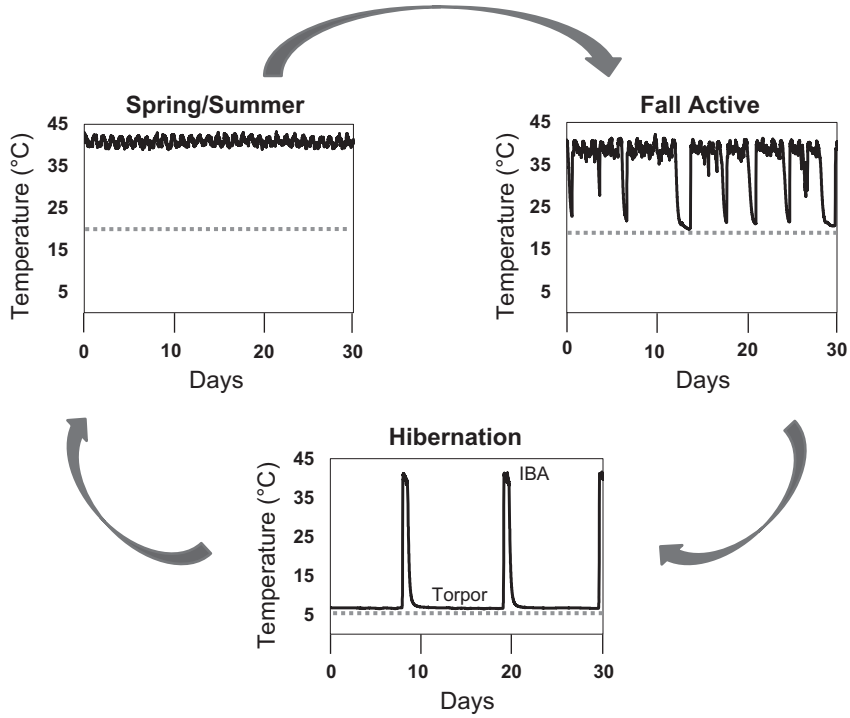

Fig. 1. Seasonal body temperature of a thirteen-lined ground squirrel. Body temperature (black, solid lines) was measured using a surgically implanted transmitter. The dashed, gray lines represent the ambient (environmental) temperature. Homeothermy, characterized by constant normothermic body temperature in spring and summer, was recorded in April. Heterothermy is seen in early fall during test bouts where squirrels drop their body temperature to room temperature (20°C) periodically, and during hibernation where hypothermic torpor is interrupted by periodic interbout arousals (IBAs), despite a constant ambient temperature of 5°C during the hibernation season.

5001) and water ad libitum. During hibernation, the squirrels were moved into an artificial hibernation chamber and kept in constant darkness at 5–7°C with water ad libitum but no food.

Four collection points were used in this study: prehibernation (fall active; FA), torpor (TOR), IBA, and post-hibernation (spring active; SP). A complete synopsis of the experimental collection points can be found in Schwartz et al. (50). An equal number of males and females were killed at each collection point. All animals were deeply anesthetized with 5% isoflurane and killed by decapitation prior to tissue collection. BAT samples were taken from the axillary pad. Whole BAT axillary pads were dissected from the surrounding tissues, cleaned of any contaminating tissue, and, for mitochondrial DNA copy number and Western blots, were flash frozen in liquid nitrogen and stored at −80°C until processing. For mitochondrial bioenergetics, separate animals were used, and dissected BAT pads and liver lobes were immediately placed in ice-cold mitochondria isolation buffer (MIB; 250 mM sucrose, 1 mM EGTA, 5 mM HEPES, pH ~7.4).

Mitochondrial DNA and Nuclear DNA Quantification via Quantitative PCR

DNA was isolated from frozen BAT samples from $n = 6$ of TOR, IBA, and SP, and $n = 9$ (6 females and 3 males) of FA using TRIzol reagent (Invitrogen, Carlsbad, CA), and 0.101 ml 1-bromo-3-chloropropane/1 ml TRIzol, according to manufacturer's instructions. Prior to DNA precipitation, samples were sonicated to ensure unbiased extraction of nuclear and mitochondrial DNA (39). Primer sequences from unique mitochondrial segments (COX2, cytochrome-*c* oxidase subunit II; ND1, NADH dehydrogenase subunit 1) and single copy nuclear genes (ACTA1, actin α1; B2M, β-2-macroglobulin) were designed following the protocol of Malik et al. (39) and were synthesized by Integrated DNA Technologies (Coralville, IA). Primer sequences are as follows: COX2 (forward: 5′-AGCCCCCGGAGATCTACGACT-3′ and reverse: 5′-CGGCCTGGGATGGCATCTGT-3′); ND1 (forward: 5′-TGTCCCAATCTTAGTAGCCATAGCCTT-3′ and reverse: 5′-TGCGTCAGCAAATGGTTGGAGT-3′); ACTA1 (forward: 5′-AAGACGCCAGCCGCGGTAAC-3′ and reverse: 5′-CTTGCTCTGGGCCTCGTCGC-3′); and B2M (forward: 5′-ATACCCGGCACCCGGCTGAG-3′ and reverse: 5′-AGAGAGGTCCGACTGCTCGACT-3′).

Target-specific standards for quantitative PCR (qPCR) were made by performing standard PCR reactions for each primer set using Amplitaq gold 360 Hot start PCR master mix (Applied Biosystems, Foster City, CA). The PCR products were then purified using QIAquick PCR purification kit (no. 28104; Qiagen, Germantown, MD) and were quantified by measuring the absorbance at 260 nm with a Nanodrop ND1000. Quantitative PCR was performed with individual mitochondrial and nuclear primers on RotorGene3000 (Qiagen) using SYBR Green Master Mix (Applied Biosystems) in accordance with the procedure of Lutfalla and Uze (37). Each sample was run in duplicate along with a 5-point, 10-fold serial dilution of target-specific standard. Crossing threshold values were derived following the procedures of Hampton et al. (24), and copy numbers of target-specific sample DNA were calculated using each target-specific standard curve. These values were used to calculate the ratio of COX2:ACTA1 and ND1:B2M, or mitochondrial to nuclear DNA.

Western Blot Analysis

Approximately 100 mg of BAT tissue was homogenized in 1 ml radioimmunoprecipitation (RIPA) buffer (150 mM NaCl, 1.0% Triton x-100, 0.5% sodium deoxycholate, 0.1% SDS, 50 mM Tris, pH 8.0) containing 10 μl/ml protease and phosphatase inhibitors using a Tissue-Tearor motor-driven homogenizer (BioSpec, Bartlesville, OK) fitted with a 7-mm probe. Protein concentration was determined using the Pierce BCA protein assay kit (ThermoFisher Scientific, Rockford, IL). The samples were diluted to 1 μg/μl in Laemmli buffer (final: 2% SDS, 100 mM DTT, 10% glycerol, 0.001% bromophenol blue, 62.5 mM Tris, pH 6.8). Samples, 15 μg/lane ($n = 2$), were loaded on a 12% SDS-PAGE mini gel and separated by electrophoresis at 180 V for 40 min. Proteins were transferred onto nitrocellulose membranes in Tris-glycine buffer (25 mM Tris, 190 mM glycine) with 20% methanol at 30 V, 4°C for 12 h. The membranes were stained with Ponceau S (P7170; Sigma, St. Louis, MO) to evaluate transfer and verify equal protein loading in each lane, followed by destaining with TBST [150 mM CaCl, 0.1% (vol/vol) Tween 20, 50 mM Tris, pH 7.5] for 10 min and blocked overnight on a shaker at 4°C with 3% BSA in

TBST. The membranes were briefly rinsed with TBST and then incubated with a primary anti-UCP1 antibody (ab10983; Abcam, Cambridge, MA) diluted 1:8,000 in TBST with 0.3% BSA at room temperature for 2 h. Membranes were rinsed twice quickly with ~30 ml TBST and then washed for 15 min on a shaker with ~20 ml TBST. The membranes were briefly rinsed two more times with TBST and then incubated at room temperature with a goat-anti rabbit secondary antibody diluted at 1:20,000 in TBST with 0.3% BSA. The secondary antibody was removed, and the membranes were washed the same as for the primary antibody. UCP1-reactive protein was detected by chemiluminescence using SuperSignal West Pico (ThermoFisher Scientific; no. 34080) and visualized using a Chemidoc XRS system (Bio-Rad, Hercules, CA). The images were exported as uncompressed JPG files, and relative quantitation was performed by densitometry using ImageJ software (48) on the ~34-kDa band. Secondary bands at ~45 and ~75 kDa were also present on the membranes. A common loading control lane was included on all membranes and used to normalize protein amounts between blots. Protein amount was normalized to total protein loading per lane determined by densitometry of the middle one-third of each lane between the largest and smallest visible bands.

Mitochondrial Isolation

Isolation of mitochondria via differential centrifugation was adapted and modified from Cannon and Nedergaard (8), Li and Graham (34), and Silva and Oliveira (52). Left axillary BAT pads were blotted and weighed for determination of wet mass. BAT pads and liver lobes were immediately rinsed in ice-cold mitochondria isolation buffer (MIB; 250 mM sucrose, 1 mM EGTA, 5 mM HEPES, pH ~7.4). The tissues were minced on ice and homogenized with 10 passes in 30 ml MIB + 0.1% fatty acid-free BSA using a rotating loose-fitting Teflon pestle. The homogenate was filtered through three layers of gauze and centrifuged at 1,000 *g* for 10 min at 4°C. Floating lipid was aspirated from the supernatant, which was transferred to a new prechilled centrifuge tube and centrifuged at 500 *g* for 10 min at 4°C. Any additional floating lipid was aspirated from the supernatant, which was transferred to a new prechilled centrifuge tube and centrifuged at 10,500 *g* for 10 min at 4°C. The supernatant was decanted, and any lipid adhering to the tubes was carefully removed using KimWipes. The pellet was resuspended in 30 ml of ice-cold wash buffer (WB; 250 mM sucrose, 5 mM HEPES, pH 7.4) + 0.1% fatty acid-free BSA and was centrifuged at 12,000 *g* for 10 min at 4°C. The supernatant was decanted, and the mitochondrial pellet was resuspended in 30 ml of ice-cold WB and centrifuged at 12,000 *g* for 10 min at 4°C. The final liver mitochondrial pellet was transferred to a prechilled Eppendorf tube. The final BAT mitochondrial pellet was aliquoted and transferred to two prechilled Eppendorf tubes. One tube of purified BAT mitochondria was frozen at −80°C until further proteomics analyses, while the second tube was kept on ice until assayed for mitochondrial respiration. The protein concentrations of isolated mitochondria were determined by BCA protein assay (Pierce BCA protein assay kit; ThermoFisher Scientific, Rockford, IL), according to the manufacturer's protocol, using BSA as a standard.

In Vitro Mitochondrial Respiration

Mitochondrial respiration measurements were performed directly after the mitochondrial isolation at 25°C. Mitochondrial respiration rates were measured using a Clark-type oxygen electrode (Hansatech Instruments, Norfolk, UK), in 0.5 or 1 ml of respiration buffer (135 mM sucrose, 65 mM KCl, 5 mM KH_2PO_4, 2.5 mM $MgCl_2$, 5 mM HEPES, pH 7.2–7.4), at 25°C while undergoing constant stirring. Unless otherwise stated, all compounds were dissolved in dH_2O.

BAT mitochondria were added in a final concentration of 0.5 mg protein/ml. Maximal flux through various segments of the electron transport chain (ETC) were determined under nonphosphorylating (state 4; Ref. 13) conditions with the addition of ADP (200 nM), using specific substrates and inhibitors (62). Flux through complexes I–IV was measured using 5 mM of glutamate/malate. Succinate (SUC; 5 mM) and glycerol-3-phosphate (G3P; 5 mM) were added to stimulate flux through complexes II–IV and complexes III and IV, respectively. Ascorbate (Asc; 5 mM) and *N,N,N′,N′*-tetramethyl-*p*-phenylenediamine (TMPD; 10 mM) were added subsequently to measure flux through complex IV. Rotenone (2 mM, dissolved in ethanol; an ETC complex I inhibitor) was added to the mitochondrial suspension before SUC to prevent reverse electron flow. Malonate (10 mM) was added before the addition of G3P to inhibit complex II, and antimycin A (2 μM) was added before the addition of Asc/TMPD to inhibit complex III. At the end, oligomycin (1 μg/ml, dissolved in ethanol; an ATPase inhibitor) was added to ensure state 4 respiration rates were being measured.

Temperature profile measurements were performed directly after the seasonal measurements (maximum 6 h) at 5, 13, 21, 29, and 37°C. A range of temperatures was chosen to mimic an arousal from torpor to IBA. BAT and liver mitochondria were added to a final concentration of 0.5 mg protein/ml. Maximal flux through complex II was determined under state 4 and state 3 (phosphorylating; 13) conditions with the addition of ADP (200 nM) in BAT and liver mitochondria, respectively. Before SUC was introduced (5 mM), rotenone (2 mM, dissolved in ethanol) was added to prevent reverse electron flow. Some temperatures have low sample sizes due to not obtaining many BAT mitochondria during SP (and having to aliquot for proteomics). Temperature coefficients (Q_{10}) were also calculated for both BAT and liver mitochondria. For Q_{10} analyses, T_2 (the second temperature) was set at 37°C, and R_2 (the second rate measurement) corresponded to the average respiration rate at 37°C (18, 57).

Protein Extraction and iTRAQ Labeling

All proteomic experiments were performed at the University of Minnesota Center for Mass Spectrometry and Proteomics (Minneapolis, MN) and were adapted from Vermillion et al. (58). Frozen isolated BAT mitochondria from SP ($n = 3$), IBA ($n = 3$), and TOR ($n = 2$) were used for iTRAQ proteomics. The mitochondria were reconstituted in PBS, vortexed briefly, and then sonicated at 30% amplitude for 7 s with a Branson Digital Sonifier 250 (Branson Ultrasonics, Danbury, CT). Each sample was placed in a Barocycler NEP2320 (Pressure Biosciences, South Easton, MA) and was cycled between 35 kpsi for 30 s and 0 psi for 15 s for 40 cycles at 37°C. The samples were alkylated with 8 mM methylmethanethiosulfonate (MMTS) at room temperature for 15 min. Two aliquots for each sample were taken for protein concentration determination by Bradford assay. Afterward, a 100-μg aliquot of each sample was transferred to a new 1.5-ml microfuge tube and brought to the same volume with protein extraction buffer plus 8 mM MMTS. All samples were trypsin digested overnight for 16 h at 37°C and then frozen at −80°C for 0.5 h and dried in a vacuum centrifuge. Each sample was cleaned with a 4 ml Extract Clean C18 SPE cartridge from Grace-Davidson (Deerfield, IL). Elutants were vacuum dried and resuspended in dissolution buffer (0.5 M triethylammonium bicarbonate, pH 8.5) to a final 2 μg/μl concentration. One set of 8-plex iTRAQ reagents was used for labeling the eight samples in the experiment. Forty micrograms of each sample was labeled with iTRAQ reagent per manufacturer's protocol (AB Sciex, Foster City, CA). Equal amounts of protein were combined from one male and one female for each time point. The peptides derived from the three spring samples were labeled with 113, 114, and 115; three IBA samples were labeled with iTRAQ reagents 116, 117, and 118; and iTRAQ 119 and 121 were used to label the two torpor samples. After labeling, the samples were multiplexed together and vacuum-dried. The multiplexed samples were cleaned with a 4-ml Extract Clean C18 SPE cartridge, and the elutants were dried in a vacuum centrifuge.

Liquid Chromotography and Tandem Mass Spectrometry (LC-MS/MS)

The iTRAQ-labeled samples were resuspended in Buffer A (20 mM ammonium formate pH 10 in 98:2 water:acetonitrile) and fractionated offline by high pH C18 reverse-phase chromatography (59). A Shimadzu Promenance HPLC (Shimadzu, Columbia, MD) was used with a C18 XBridge column, 150 mm × 2.1 mm internal diameter, 5-μm particle size (Waters, Milford, MA). The flow rate was 200 μl/min with a gradient from 2 to 35% Buffer B (20 mM ammonium formate, pH 10 in 10:90 water:acetonitrile) over 60 min, followed by 35–60% over 5 min. Fractions were collected every 2 min, and UV absorbance was monitored at 215 nm and 280 nm. Peptide containing fractions were divided into two equal numbered groups, "early" and "late". Concatenated samples were dried in a vacuum centrifuge, resuspended in load solvent (98:2:0.01, water:acetonitrile:formic acid), and 1–1.5 μg aliquots were run on a Velos Orbitrap mass spectrometer (ThermoFisher Scientific, Waltham, MA), as described previously (41), with the exception that the higher-energy collisional dissociation (HCD) activation energy was 20 ms.

Bioinformatic Analysis

The MS/MS spectra were searched using a customized ground squirrel database generated from the NCBI-annotated thirteen-lined ground squirrel genome merged with RNA-seq-data generated in the laboratory (23), along with the contaminants database using Paragon Alogirithm (v. 4.5.0.0) search engines in ProteinPilot (v. 4.5; AB-Sciex, Foster City, CA). The precursor mass window was set to sub-parts per million, and MS/MS error tolerance was set at 0.1 Da with up to one missed tryptic cleavage. Eight-plex iTRAQ peptide labeling and cysteine MMTS alkylation were set as fixed modifications. The search effort was thorough, and the ID focus was set for biological modifications. All peptides were identified with at least a 95% confidence interval value, as specified by the Paragon Algorithm in ProteinPilot, and less than a 1% false discovery rate (FDR) based on target-decoy database searches. Relative quantification of proteins was determined by ProteinPilot in a normalized $\log_{10}$-based relative iTRAQ ratio format, with iTRAQ 113, 114, and 115 as the reference denominators. Multiple hypothesis testing for quantitative analysis of these samples were accounted for using the Sciex ProteinPilot Descriptive Statistics Template (PDST) outputs to estimate the threshold of P values to be used for differential analysis. On the basis of PDST template calculations, proteins were considered differentially expressed relative to the reference denominator if they had at least two unique peptides, an experiment-wide FDR of no more than 1%, and a P value ≤ 0.001. ProteinPilot defines P value as a measure of the certainty that the average ratio randomly differs from 1. Significant differences must be present in two or three of the samples in each time point, and show the same trend. Differentially expressed proteins were submitted into the Database for Annotation, Visualization and Integrated Discovery (DAVID; Refs. 29, 30), and literature searches were performed to highlight proteins associated with various mitochondrial functions. Significance of the DAVID enrichment score was set to greater than 1.3 (26).

Data Analysis

Statistical analysis was carried out on the mtDNA copy number, BAT pad mass, and mitochondrial respiration data using JMP Pro 11 statistical software. Significant differences between groups were analyzed using one-way ANOVA and were considered significant at $P < 0.05$. Temperature assays were analyzed using a two-way ANOVA, where differences between groups and temperature were considered significant at $P < 0.05$. Significant results from ANOVA tests were further analyzed using a Tukey's honestly significant difference (HSD) test to find means that were significantly different from each other ($P < 0.05$). P values presented below are Tukey's HSD values.

RESULTS

BAT Mass and Recruitment

Qualitatively, we have observed that axillary BAT pad mass in thirteen-lined ground squirrels increases prior to the hibernation season. To further investigate these observations, the masses of left axillary BAT pads were measured immediately after excision. Means of BAT mass (g) ± SE for spring (SP), fall (FA), torpor (TOR), and interbout arousal (IBA) were 0.41 ± 0.03, 0.89 ± 0.05, 1.17 ± 0.05, and 0.98 ± 0.07, respectively. BAT mass was significantly lower in SP compared with FA, TOR, and IBA ($P < 0.0001$, Fig. 2*A*). TOR also showed significantly higher BAT mass compared with FA ($P < 0.01$). The mass of axillary pads begins to increase during FA in preparation for hibernation and is heaviest during the hibernation season (TOR and IBA).

In addition, BAT mitochondrial abundance was determined via mitochondrial DNA (mtDNA) to nuclear DNA (nuDNA) ratio measurements across the circannual cycle (Fig. 2*B*). Similar to wet mass results, SP animals had the lowest mtDNA copy number compared with FA, TOR, and IBA states ($P < 0.05$), suggesting an overall decrease in BAT mitochondrial abundance during SP. This trend in BAT mitochondrial abundance was initially observed in UCP1 mRNA levels, with UCP1 transcripts significantly higher in TOR and IBA compared with spring (23). Protein quantification of UCP1 was determined via Western blot analysis (Fig. 2*C*). Although not significant, the same trend identified in BAT pad mass and mtDNA copy number was also observed measuring UCP1 protein, with the hibernation time points containing more UCP1 protein in BAT (Fig. 2*C*).

BAT and Liver Mitochondrial Respiration

Individual complexes of the ETC in BAT mitochondria were interrogated across the circannual cycle of the thirteen-lined ground squirrel. On the basis of fuel utilization and specific ETC inhibitors, no significant differences were identified at complexes I, III, or IV; however, significant differences were observed at complex II. Fueled with succinate (SUC), complex II of isolated BAT mitochondria from SP had significantly lower respiration rates compared with FA, TOR, and IBA ($P < 0.05$, Fig. 3).

Additional investigation was done on the effects of temperature on mitochondrial metabolism, using SUC as a fuel. There were no significant differences at any temperature between SP, FA, TOR, and IBA in BAT mitochondria (Fig. 4*A*). However, liver mitochondria showed sensitivity to temperature across the year, having lowest rates during TOR at all five temperatures assayed (Fig. 4*B*). Specifically, liver respiration rates during TOR were significantly lower than FA respiration rates at all five temperatures ($P < 0.05$; Fig. 4*B*), while FA contained the highest respiration rates at all five temperatures ($P < 0.01$; Fig. 4*B*). Additionally, TOR had lower respiration rates compared with SP at 29°C, 21°C, and 13°C ($P < 0.05$), and compared with IBA at 29°C, 13°C, and 5°C ($P < 0.05$; Fig. 4*B*).

Comparisons between normothermic and torpid animals were performed to understand whether decreases in metabolism are due to passive thermal effects or whether metabolism

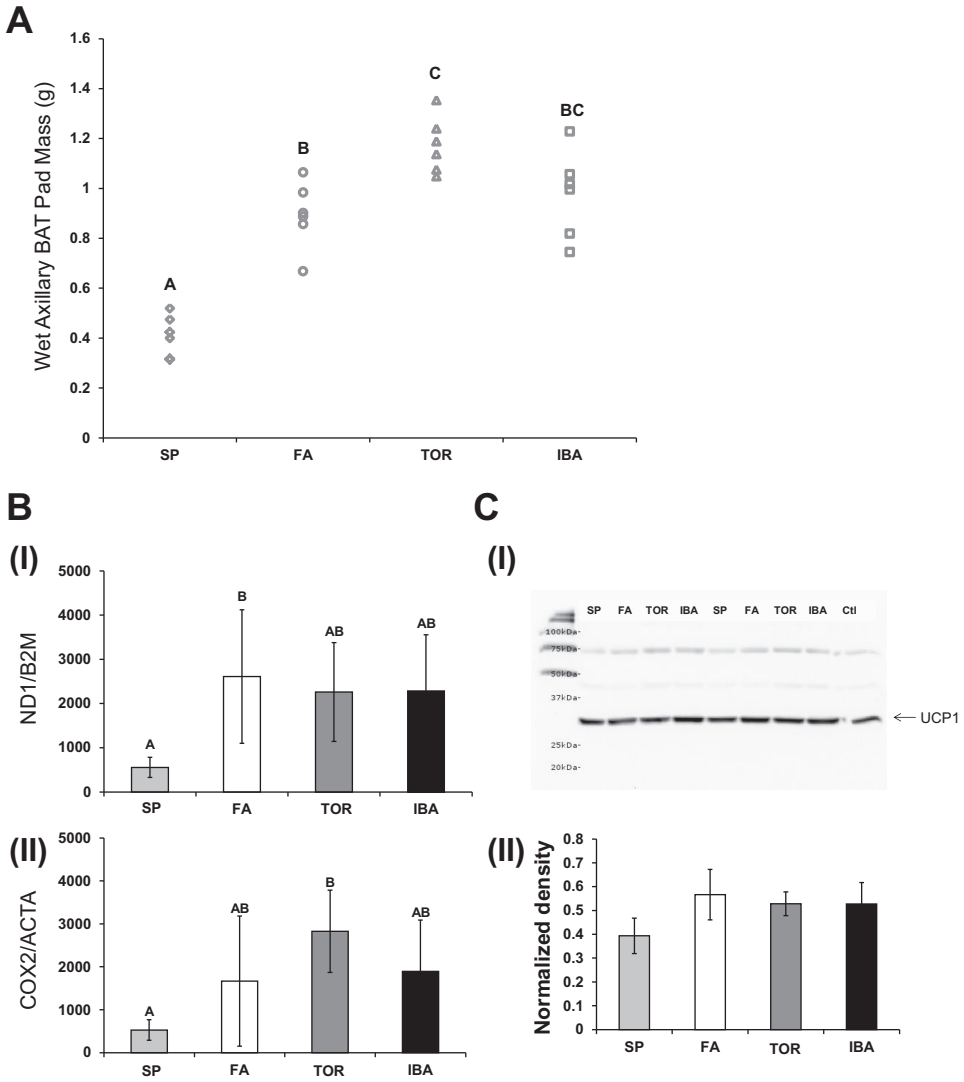

Fig. 2. Relative mitochondrial content of brown adipose tissue (BAT) across the circannual cycle. *A*: seasonal BAT pad mass was measured from the left axillary pad between SP, FA, TOR, and IBA time points ($n = 6$). Individual animals are represented by symbols. Time points that do not share the same letter are significantly different (Tukey's highly significant difference test). *B*: mitochondrial DNA (mtDNA) to nuclear DNA (nuDNA) ratios in BAT. Ratios of mitochondrial genes [*ND1* (*I*) and *COX2* (*II*)] to nuclear genes (*B2M* and *ACTA*) were quantified via quantitative PCR in ground squirrel brown adipose tissue ($n = 6$). Data are presented as means ± SE. *C*: representative Western blot (*I*) and densitometry (*II*) of ~30 kDa UCP1 band. The expression of UCP1 protein was determined via Western blot analysis. Fifteen micrograms of BAT protein homogenate was loaded in each lane ($n = 2$). ImageJ (47) was used to measure the density of the ~30-kDa band from Western blots using anti-UCP1 antibody. Bands from each of the two blots were normalized to a common lane (Ctl) with 15 μg of pooled BAT homogenate. No significant differences in UCP1 abundance were observed. Error bars show means ± SE. SP, spring active; FA, fall active; TOR, torpor; IBA, interbout arousal; Ctl, control; UCP1, uncoupling protein 1.

is actively inhibited. At 37°C, there was no difference in BAT mitochondrial respiration rates of samples taken from animals during normothermic and torpor seasons, but liver mitochondrial respiration rates from FA samples were higher than those in TOR samples ($P < 0.01$; Fig. 4*B*). At 5°C, again, there is no difference in BAT mitochondrial respiration rates taken from animals during normothermic and torpor seasons; however, BAT respiration rates at 5°C are significantly lower than rates at 37°C ($P < 0.0001$; Fig. 4*A*). For liver, at 5°C, FA and IBA samples have higher respiration rates than TOR samples ($P < 0.05$; Fig. 4*B*), and liver respiration rates at 5°C are significantly lower than rates at 37°C ($P < 0.0001$; Fig. 4*B*). On the basis of Q_{10} analyses, the majority of BAT and liver Q_{10} values were between 2 and 3, suggesting that passive effects play a major role in reducing metabolism (22, 53, 55). However, when Q_{10} is greater than 3, active processes are also involved in regulating metabolic suppression (18, 55). The higher Q_{10} values were typically obtained at the lower temperatures in both BAT and liver, with a trend toward decreasing Q_{10} values as the temperature approached 37°C (Tables 1 and 2). For SP BAT, while R_2 and T_2 still corresponded to 37°C values, respiration rates were only available for 5°C and 13°C and were 3.0 and 2.6, respectively. For liver, the same trend as BAT was seen with higher Q_{10} values obtained at lower temperatures (Tables 1 and 2).

BAT Mitoproteomics

Overall, 778 BAT mitochondrial proteins were positively identified in the thirteen-lined ground squirrel across the hibernation and spring time points. The top mitochondrial proteins are encoded by many transcripts that were also highly expressed in the BAT transcriptome (23), such as UCP1 (Fig. 5). Of the 778 total proteins, 106 were differentially expressed according to the criteria outlined in METHODS (Supplemental Table S1). In this proteomic study, the hibernation time point (HIB) is a combination of data from TOR and IBA. As a result, 56 proteins showed highest expression in HIB, while 48 proteins showed highest expression in SP compared with HIB. UCP1 did not make the differential expression cut-off criteria; however, it did show the same trend as the BAT transcriptome and Western blot analyses, with UCP1 showing high protein levels in HIB.

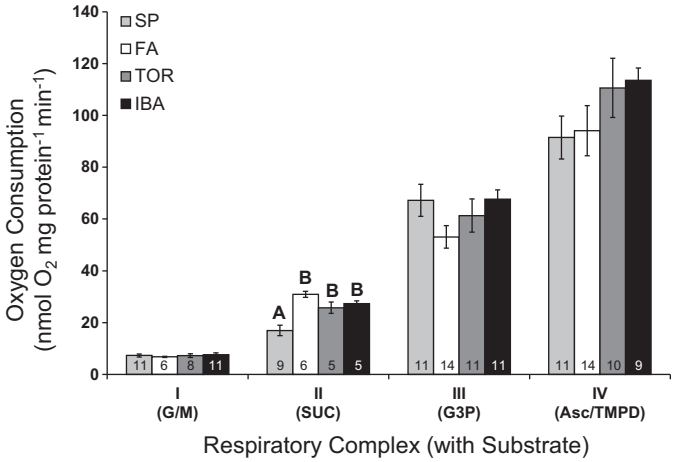

Fig. 3. Seasonal respiration rates in isolated BAT mitochondria. State 4 (nonphosphorylating) respiration rates were measured at complexes I–IV. Time points at complex II (SUC) that do not share the same letter are significantly different (Tukey's HSD). The number of samples for each value is indicated in each bar. Data are expressed as means ± SE. Asc/TMPD, ascorbate/TMPD; G/M, glutamate/malate; G3P, glycerol-3-phosphate; SUC, succinate; TOR, torpor.

Functional Analysis of Mitoproteomics

To further analyze the differentially expressed proteins, DAVID functional annotation clustering was used (31). As expected, both data sets (highest expression in HIB and highest expression in SP) contained the largest enrichments for mitochondria-located proteins (Tables 3 and 4). Not only do these top enrichments validate our mitochondrial isolation, but they also inform us on the important localities of proteins between HIB and SP. For example, HIB had the highest enrichment for proteins found in the mitochondrial membranes, while SP proteins had the highest enrichment for the mitochondrial matrix.

Proteins showing highest expression in HIB. Overall, pathways that showed highest enrichment of BAT mitochondrial proteins during HIB dealt with lipid oxidation and fatty acid metabolism (Table 3). Fatty-acyl CoA mitochondrial transport proteins, such as CPT1B, CPT2, and SLC25A20, had highest expression during HIB. These proteins are also important in the carnitine shuttle. There is also more efficient mitochondrial protein trafficking during HIB as the inner membrane translocase was enhanced by more abundant motor and associated proteins (TIMM50 and TIMM44). Additionally, β-oxidation of fatty-acyl CoA was also enriched (CPT1B, CPT2, ACADS, ECHS1, DECR1, CRAT, HSD17B4, HADHA, HADHB). Hibernation also favors isocitrate metabolism compared with spring, with isocitrate conversion to α-ketoglutarate being enhanced (IDH3B, IDH3G, IDH2) and an increase of NADH shuttling into the ETC. In fact, Hindle and Martin (26) see the same enhancement of catabolism of isocitrate during HIB and validated this through an IDH3 assay where they showed ~80% increase in IDH3 in IBA compared with summer active animals. Additionally, coenzyme binding proteins (D2HGDH, AIFM1, ACADS, IDH3B, DECR1, OGDH, and HADHB) are also enhanced during HIB in BAT mitochondria, allowing for essential metabolic enzymatic reactions to proceed (i.e., TCA cycle and β-oxidation).

Proteins showing highest expression in SP. Unlike HIB, where fatty acid metabolism and β-oxidation proteins are enriched, SP contains mitochondrial proteins enriched for acetyl-CoA and pyruvate metabolism (Table 4). This further validates the body-wide switch in metabolism from lipid to carbohydrate in the spring in the thirteen-lined ground squirrel (10, 15). Further recognition of this metabolic switch is through the enrichment of TCA cycle enzymes (Table 4). Unlike in HIB, where CS and IDH enzymes are enhanced, succinate metabolism is enriched (SDHA and SDHB). Additionally, citrate to isocitrate (ACO2) is enhanced in SP, and these observations were also seen by Hindle and Martin (26). Lastly, fatty acid binding is decreased during SP, supported again by the decrease in lipid metabolism outside of hibernation.

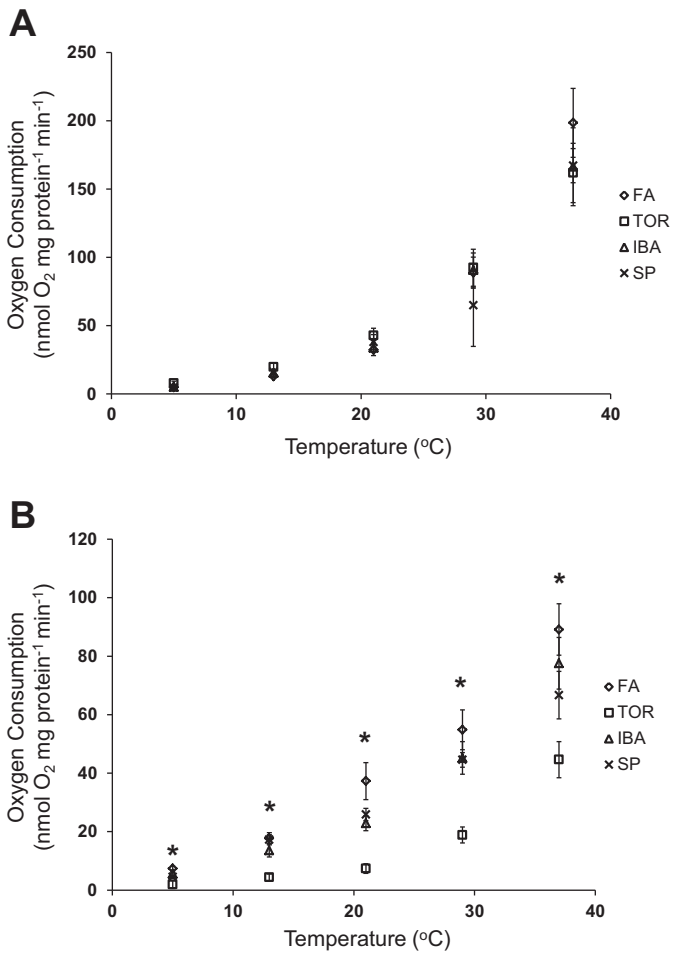

Fig. 4. Temperature effects of respiration rates in isolated BAT and liver mitochondria. *A*: respiration rates of BAT mitochondria at different temperatures. State 4 respiration rates were measured at complex II using succinate as fuel at five different temperatures (5°C, 13°C, 21°C, 29°C, and 37°C). Data are expressed as means ± SE; $n = 6$ for each time point at each of the five temperatures (except for SP, which had $n = 2$ for 21°C and $n = 2$ for 29°C). *B*: respiration rates of liver mitochondria at different temperatures. State 3 (phosphorylating) respiration rates were measured at complex II, using succinate as a fuel at five different temperatures (5°C, 13°C, 21°C, 29°C, and 37°C). *Significant differences between two or more seasons at the given temperature (Tukey's HSD test). Data are means ± SE; sample sizes at each of the five temperatures for SP, FA, TOR, and IBA are $n = 7$, $n = 8$, $n = 5$, and $n = 8$, respectively. Data are expressed as means ± SE.

Table 1. *Mean respiration rate and Q_{10} values for BAT mitochondria across the circannual cycle for a temperature range of 37°C to 5°C*

	Q_{10} values for temperature range of 37°C to 5°C	Q_{10} values for temperature range of 37°C to 13°C	Q_{10} values for temperature range of 37°C to 21°C	Q_{10} values for temperature range of 37°C to 29°C
SP	3.04	2.65	n/a	n/a
FA	3.18	3.13	3.12	2.73
TOR	2.57	2.40	2.30	2.01
IBA	2.96	2.69	2.70	2.13

Temperature coefficients (Q_{10}) values reflect the capacity of organisms to change their metabolic rate relative to changes in temperature (each temperature compared to 37°C). The second temperature (T_2) was set at 37°C, and R_2 (the second rate measurement) corresponded to the average respiration rate at 37°C (17, 56). SP, spring active; FA, fall active; TOR, torpor; IBA, interbout arousal.

DISCUSSION

Brown adipose tissue plays an important role in nonshivering thermogenesis, as thirteen-lined ground squirrels readily arouse from torpor to IBA during hibernation. The major thermogenic function and characteristics of BAT are primarily due to mitochondria containing UCP1 that short-circuits the electron transport chain and, thereby, produces heat. Here, we investigated BAT morphology, mitochondrial proteomics, and mitochondrial respiration to evaluate components essential for BAT function during heterothermic and homothermic states. We also included the seasonal BAT transcriptome (23) to develop an understanding of how gene and protein expression correlate with function in brown adipose tissue mitochondria.

Increase of BAT Mitochondrial Abundance Allows for Enhanced Metabolic Activity

Brown adipose tissue mass is reduced in the spring, but increases during fall in preparation for hibernation. This trend in recruitment is also observed by large proteome differences between two homeothermy states in BAT compared with other tissues (20), and by increased mitochondrial membrane proteins (reviewed in Ref. 7). Unlike previous studies (26), we were able to detect many of the mitochondrial membrane proteins due to our proteomics technique using a barocycler (see METHODS for details). Rather than abundant changes in ETC proteins, structural mitochondrial proteins (i.e., membrane transporters) are increased in hibernation (26). This increase in membrane transporters allows BAT mitochondria to have an increase in fatty acid handling that accommodates the increased lipid metabolism present during hibernation (Refs. 20 and 26, reviewed in Refs. 7 and 10) (Fig. 6).

In addition to the overall mass, mitochondrial abundance in BAT increases during fall, evidenced by the mtDNA copy number results. Our mtDNA copy number results oppose previous studies, indicating similarities in mitochondrial abundance between hibernation and posthibernation periods (26). However, not only did this previous study use different primers, but they also did not take into account the possibility that mitochondrial biogenesis and recycling (19, 35, 61) may require weeks posthibernation to see any noticeable effects. This assumption is supported when comparing genes associated with mitochondrial biogenesis and the BAT transcriptome. For example, calcineurin (32) and *PGC1α* (33) are positively correlated with mitochondrial biogenesis and show significantly higher mRNA expression in BAT during hibernation (23).

Mitochondrial abundance can also be quantified by determining UCP1 levels in BAT. Initially, we observed an increase in UCP1 mRNA levels during hibernation, with UCP1 transcripts significantly higher in TOR and IBA compared to spring (23). However, the level of UCP1 mRNA can show a dramatic response (7), as the turnover rate of UCP1 protein is slow because of its requirement of mitochondrial synthesis (7). Therefore, UCP1 mRNA is a less feasible indicator of BAT recruitment because of the long time delay before modifications in UCP1 mRNA levels lead to corresponding amounts of UCP1 protein (7). Instead, the most physiologically relevant measure of both BAT recruitment and the actual thermogenic capacity change occurring during hibernation is through the quantitation of UCP1 protein directly (7). With both mitoproteomics and Western blot analyses, we identified a nominal, nonsignificant increase in UCP1 protein during HIB. This suggests that although there are more mitochondria present during hibernation (as indicated by the mtDNA copy number results), UCP1 protein levels do not increase, as the mitochondria contain the same amount of UCP1. However, with more mitochondria per cell during hibernation, the oxidative capacity of BAT is increased, and thus, more heat can be produced (Fig. 6).

Enhanced Oxidative Capacity During Hibernation Promotes Increased Heat Production

Brown adipose tissue mitochondria rely on numerous lipid reserves for fuel that are present throughout the hibernation season (20). This, in turn, allows for an increase in reducing equivalents (i.e., NADH and $FADH_2$) to shuttle into the ETC during torpor and IBA. In fact, respiration rates of BAT mitochondria at three of the four complexes are high or highest during TOR and IBA, suggesting an increase in the delivery of reducing equivalents in BAT during hibernation. The transcriptome and proteome also support this observation as levels of transcripts and proteins for ubiquinone are enhanced in TOR and IBA. For example, *COQ10A* mRNA transcript levels are significantly higher in IBA compared with spring (23). COQ10B has higher expression in HIB in the mitoproteome, and Hindle and Martin (26) show COQ5 protein is highly expressed in HIB as well. Moreover, there is no difference in BAT respiration rates between TOR and IBA, suggesting that BAT mitochondria are primed and ready during hibernation to

Table 2. *Mean respiration rate and Q_{10} values for liver mitochondria across the circannual cycle for a temperature range of 37°C to 5°C*

	Q_{10} values for temperature range of 37°C to 5°C	Q_{10} values for temperature range of 37°C to 13°C	Q_{10} values for temperature range of 37°C to 21°C	Q_{10} values for temperature range of 37°C to 29°C
SP	2.31	1.76	1.81	1.65
FA	2.17	1.96	1.72	1.84
TOR	2.62	2.55	3.09	2.95
IBA	2.28	2.06	2.14	1.96

Temperature coefficients (Q_{10}) values reflect the capacity of organisms to change their metabolic rate relative to changes in temperature (each temperature compared to 37°C). The second temperature (T_2) was set at 37°C, and R_2 (the second rate measurement) corresponded to the average respiration rate at 37°C (17, 56).

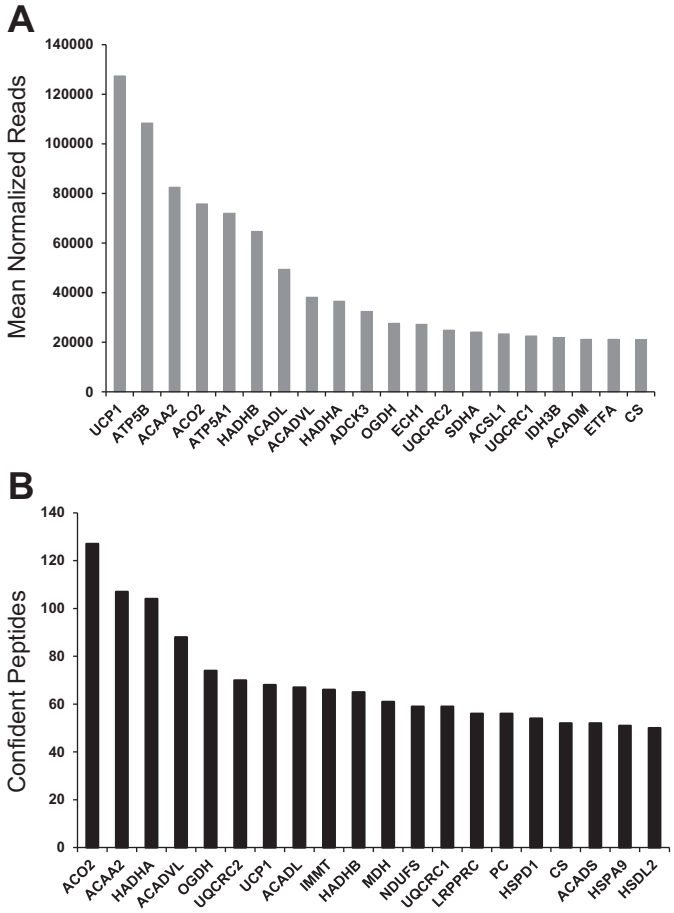

Fig. 5. Comparison of BAT transcripts (*A*) and mitochondrial proteins (*B*). Top 20 most abundant BAT transcripts (23), encoding mitochondrial proteins (*A*) were compared with the top 20 most abundant BAT mitochondrial proteins (*B*). ACAA2, 3-ketoacyl-CoA thiolase; ACADL, acyl-CoA dehydrogenase, long chain; ACADS, short-chain specific acyl-CoA dehydrogenase; ACADVL, very long-chain specific acyl-CoA dehydrogenase; ACO2, aconitate hydratase; ATP5B, ATP synthase, beta polypeptide; ATP5A1, ATP synthase, alpha subunit 1; ADCK3, aarF domain containing kinase 3; ACADM, acyl-CoA dehydrogenase; ACSL1, acyl-CoA synthetase long-chain family member 1; CS, citrate synthase; ECH1, enoyl CoA hydratase 1; ETFA, electron-transfer-flavoprotein, alpha polypeptide; HADHA, hydroxyacyl-CoA dehydrogenase/3-ketoacyl-CoA thiolase/enoyl-CoA hydratase, alpha subunit; HADHB, hydroxyacyl-CoA dehydrogenase/3-ketoacyl-CoA thiolase/enoyl-CoA hydratase, beta subunit; HSPD1, heat shock 60-kDa protein 1; HSPA9, heat shock 70-kDa protein 9; HSDL2, hydroxysteroid dehydrogenase like 2; IDH3B, isocitrate dehydrogenase 3 beta; IMMT, inner mitochondrial membrane protein; LRPPRC, leucine-rich PPR-motif containing; MDH, malate dehydrogenase; NDUFS, NADH dehydrogenase, Fe-S protein; OGDH, oxoglutarate dehydrogenase; PC, pyruvate carboxylase; SDHA, succinate dehydrogenase complex, subunit A; UCP1, uncoupling protein 1; UQCRC2, ubiquinol-cytochrome-*c* reductase core protein II; UQCRC1, ubiquinol-cytochrome-*c* reductase core protein I.

produce heat once the norepinephrine signal is present. These results suggest an increase in BAT mitochondrial metabolism and efficiency in heat production during hibernation (Fig. 6).

To further illustrate the thermogenic capacity of BAT, liver mitochondria were assayed to compare mitochondrial metabolism at various temperatures. Unlike liver mitochondria, where the greatest suppression of respiration rates occurs during torpor at all five temperatures, BAT mitochondria show no suppression of respiration during torpor at any temperature compared with other seasons. Additionally, there were no differences in BAT mitochondrial respiration rates at 37°C and 5°C in samples taken from animals during normothermic and torpid seasons, suggesting passive thermal effects (i.e., temperature changes) are sufficient to explain decreases in metabolism at 5°C (5). Liver mitochondria showed both passive and active regulated changes to lower metabolism during torpor, as respiration rates between FA, IBA, and TOR were different at both 37°C and 5°C. This result has also been observed in previous studies using hamsters and ground squirrels (reviewed in Ref. 56). BAT mitochondria isolated from fall animals have a greater reliance on active processes for function at lower temperature, suggesting there may be intrinsic regulation present in BAT mitochondria that allows function to remain the same across the circannual cycle. Overall, unlike liver mitochondria in thirteen-lined ground squirrels, BAT mitochondria are able to function at the same capacity, regardless of season.

Spring Contains Enhanced Mitochondrial Protein and Function

While stored lipids serve as the primary fuel during hibernation, an increase in carbohydrate metabolism characterizes the spring season (10). This is supported by the BAT mitoproteome, in which SP shows fewer proteins involved in fatty acid metabolism, and more proteins involved in acetyl-CoA and succinate metabolism. However, we see suppression in BAT respiration rates at complex II in the spring, using succinate as a fuel. In general, succinate metabolism is relatively simple, requiring only transport across the inner mitochondrial membrane and oxidation by ETC complex II (56). Metabolism of pyruvate derivatives, such as glutamate/malate, is more complex, and includes oxidation through the TCA cycle. Suppression of BAT mitochondrial respiration in SP is more modest with these substrates (i.e., complex I) than it is with succinate, suggesting that much of the suppression occurs at complex II.

The observed suppression of succinate-fueled respiration in spring may be caused by ETC complex II inhibition via oxaloacetate, a TCA cycle intermediate (16, 56). Upon investigating succinate-fueled respiration at complex II across different temperatures between SP, TOR, and IBA, we do not see the same suppression during SP. This suggests that the mitochondrial metabolic activity involving the TCA cycle may not be enhanced during SP in BAT (12). These functional differences in spring and hibernation suggest seasonally distinct regulation of TCA cycle intermediates. It is noteworthy that the observed seasonality will produce the most metabolically meaningful differences in concentrations of isocitrate, succinate, and oxaloacetate, all of which are able to exert allosteric or competitive effects on the respiratory activity of complex II (3, 4, 14, 26, 56).

Furthermore, the spring time point has an increase in handling the reducing equivalent $FADH_2$, which can be generated by the glycerol phosphate shuttle. The glycerol phosphate shuttle contains two components, the cytosolic glycerol-3-phosphate dehydrogenase (GDP1) and the mitochondrial form (GDP2). Levels of the glycerol phosphate shuttle and its corresponding enzymes are highest in mammalian BAT, supporting cytosolic ATP generation by NADH reoxidation (11, 46). In BAT, all energy created by oxidative phosphorylation is dissipated as heat (reviewed in Ref. 44), and since BAT

Table 3. *Differentially expressed BAT proteins showing highest expression in hibernation*

Annotation Terms	Score	Protein (Corresponding Gene Abbreviation Shown)
Subcellular location		
Mitochondrial membrane	24.04	CKMT1B, CPT2, SAMM50, NLRX1, TIMM50, OGDH, HADHA, HADHB, GOT2, SLC25A20, ACSL1, MTCH2, DNAJC11, HADH, CPT1B, ACAA2, ABCB8, IMMT, AK2, CRAT, VDAC2, SLC25A11, NNT, PHB2, PMPCA, PMPCB, PC
Mitochondrial matrix	11.13	PDPR, ACADS, CYCS, CS, AK3, ECHS1, IDH3B, OGDH, VDAC2, HADHA, HADHB, GOT2, IDH3G, PITRM1, HADH, PMPCA, PDHX, PMPCB, PC
Mitochondrial import		
Fatty acid transport	2.50	GOT2, CPT1B, SLC25A20, CPT2
Ion transport	2.50	CPT1B, SLC25A20, CPT2, NNT, AMACR, VDAC2
Transmembrane transport	2.50	CPT1B, SLC25A11, SLC25A20, CPT2, ABCB8, MTCH2, TIMM50, VDAC2
Mitochondrial metabolism		
Fatty acid metabolism/β-oxidation	10.39	ACAA2, CPT1B, CPT2, ACSL1, ACADS, ECHS1, CRAT, HSD17B4, HADH, HADHA, HADHB, DECR1
TCA cycle	4.13	IDH3G, CS, IDH2, IDH3B, OGDH, PCK2, PC
Isocitrate metabolic process	4.13	IDH3G, IDH2, IDH3B
Aerobic respiration	4.13	NNT, IDH3G, CYCS, CS, IDH2, IDH3B, OGDH
Binding and carrier activity		
Coenzyme binding	10.00	D2HGDH, AIFM1, ACADS, IDH3B, DECR1, OGDH, HADHB, NNT, IDH3G, IDH2, HADH, PDHX
NAD binding	4.13	NNT, IDH3G, IDH2, IDH3B, HADHA, HADHB
Fatty acid binding	2.77	ACADS, HADHA, HADHB
FAD binding	1.50	D2HGDH, AIFM1, ACADS
Adenyl nucleotide binding	1.45	CPT1B, D2HGDH, ABCB8, IDH3G, ACSL1, CKMT1B, AIFM1, ACADS, AK3, NLRX1, AK2, PC

Enrichments by DAVID. ″Score″ denotes DAVID enrichment score (significance set >1.3).

mitochondria have little ATP synthase, ATP production is important (9, 42). In general, GDP2 converts glycerol to glycerol-3-phosphate, which leads to transport of $FADH_2$ into mitochondria via ubiquinone for respiration (28, 42). The mitoproteome shows an enhancement of GDP2, which is further supported by high respiration rates at complex III in SP when fueled with glycerol-3-phosphate. Additionally, glycerol kinase, the enzyme that converts glycerol to glycerol-3-phosphate, is significantly higher in the spring than fall in the transcriptome (23), further suggesting an increase in $FADH_2$ handling during spring. Overall, the mitochondrial component of the glycerol phosphate shuttle is enhanced in the spring, which is likely an element of retained thermogenic capacity in spring BAT, despite reduced fatty acid metabolism and lipid reserves (26).

Integration of BAT Transcriptome, Mitoproteome, and Function

Although this study measured in vitro mitochondrial dynamics, a more complete picture of hibernator BAT was constructed due to the integration of the BAT transcriptome, mitoproteome, and functional assessments. Despite the transcriptome giving us massive depth and coverage, mRNA levels are not always correlated closely with protein abundance in living systems (14a, 17, 21, 45, 47, 60). We previously developed an approach for identifying proteins from nonmodel organisms using mass spectrometry (49), and more recently, we used a proteogenomic approach to identify differentially expressed proteins in the heart (58) and skeletal muscle (1) of a hibernating ground squirrel. In this study, we measured

Table 4. *Differentially expressed BAT proteins showing highest expression in spring*

Annotation Terms	Score	Protein (Corresponding Gene Abbreviation Shown)
Subcellular location		
Mitochondrial membrane	6.33	GPD2, GCDH, SHMT2, SUCLG1, NDUFA7, ACAT1, SLC25A12, ACADVL, SDHA, SDHB, SLC25A3, ETFDH, HSPD1
Mitochondrial matrix	17.01	BCKDHA, GCDH, SHMT2, ACO2, SUCLG2, SUCLG1, LARS2, ACAT1, ACADVL, DBT, ACSS1, LONP1, MUT, IVD, ALDH4A1, HSPD1, PCCB, OAT, ETFB, LRPPRC, PCCA, ACSM5, ETFA
Mitochondrial metabolism		
acetyl-CoA metabolism	5.15	SDHA, SDHB, ACSS1, ACO2, SUCLG2, MLYCD, SUCLG1
Succinate metabolism	5.15	SDHA, SDHB, ACO2, SUCLG2, SUCLG1, SDHA, SDHB
Fatty acid metabolism	3.31	ACADVL, GCDH, ALDH7A1, ACAT1, ALDH9A1, ACSS1
Pyruvate metabolism	3.31	ALDH7A1, ACAT1, ALDH9A1
Binding and carrier activity		
Conenzyme Binding	6.06	SDHA, ACADVL, DBT, GCDH, ALDH6A1, IVD, ETFDH, ACAD10, ETFA
FAD binding	6.06	GPD2, SDHA, ACADVL, GCDH, IVD, ETFDH, ACAD10, ETFB, ETFA
Adenyl nucleotide binding	4.06	ACTB, GCDH, SUCLG2, LARS2, ACSS3, ACSF2, SDHA, ACADVL, TRAP1, ACSS1, LONP1, IVD, ETFDH, HSPD1, PCCB, EHD2, ACAD10, PCCA, ACSM5, ETFA
Electron transport chain		
OXPHOS	3.33	SLC25A12, SDHA, SDHB, NDUFA7, ETFDH, ETFB, ETFA

Enrichments by DAVID. ″Score″ denotes DAVID enrichment score (significance set >1.3).

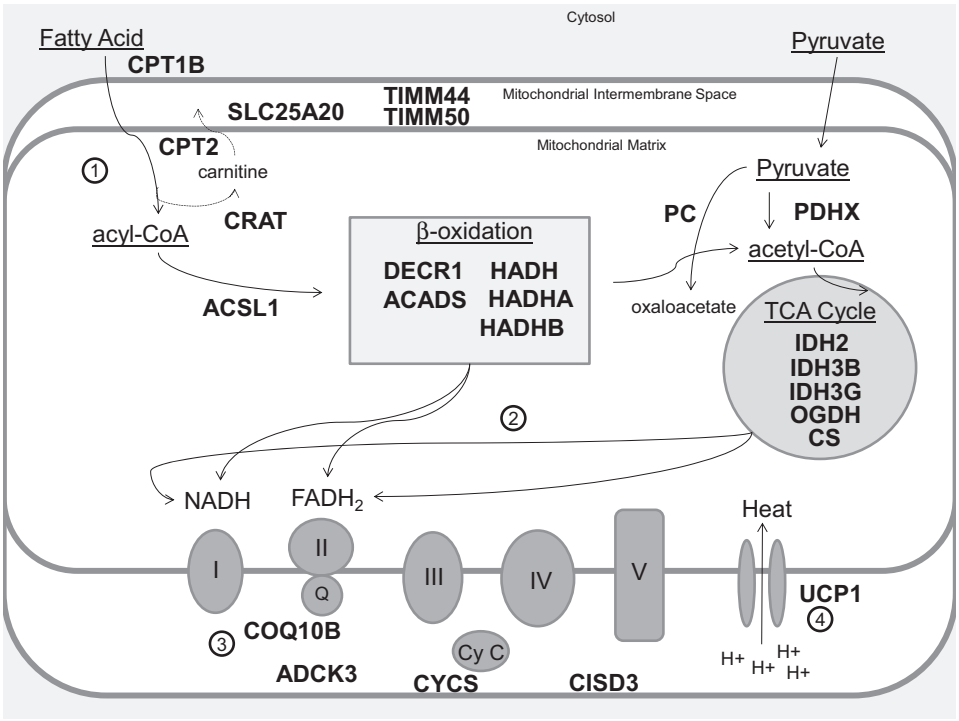

Fig. 6. Mitochondrial model of BAT proteins and function during hibernation. The results of this study were used to construct a functional model of BAT mitochondria during hibernation (torpor and IBA). The proteins shown in the model are proteins that show highest expression during hibernation. Numbered steps (circled 1–4) in this model are the following: *1*) Increases in membrane and transport proteins during hibernation allow for an increase in fatty acid handling in BAT mitochondria. *2*) Along with fatty acid handling, an increase in mitochondrial metabolism associated with β-oxidation and TCA cycle are present during hibernation. This is evidenced by enhancements of both transcripts (23) and proteins associated with the two pathways. This metabolic enhancement allows for an increase in reducing equivalents (i.e., NADH and $FADH_2$) to flow into the electron transport chain (ETC), evidenced again by the increase in respiration during hibernation. *3*) The increase in reducing equivalents shuttling through the ETC is indicated by enhanced respiration rates through the various complexes of the ETC during hibernation. This is shown through the increased maximal respiration rates of various ETC complexes during hibernation, along with an enhancement of proteins that aid in the transfer of electrons through the ETC (see Table 1). *4*) The enhancements of all the various mitochondrial aspects (nos. 1–3) allow for an increase in heat production via UCP1 during hibernation. This rapid and efficient heat production aids in the rewarming process of arousal from torpor to IBA. [Note: UCP1 did not make the differential expression cutoff (see METHODS for details); however, it does have the trend of being more highly expressed during hibernation compared with spring.] ACADS, short-chain specific acyl-CoA dehydrogenase; ACSL1, long-chain-fatty-acid–CoA ligase 1; ADCK3, aarF domain containing kinase 3; CISD3, CDGSH iron-sulfur domain 3; COQ10B, coenzyme Q10 homology B; CPT1B, carnitine palmitoyltransferase 1B; CPT2, carnitine O-palmitoyltransferase 2; CRAT, carnitine O-acetyltransferase; CS, citrate synthase; CYCS, cytochrome *c*, somatic; DECR1, 2,4-dienoyl-CoA reductase; HADH, hydroxyacyl-coenzyme A dehydrogenase; HADHA, trifunctional enzyme subunit alpha; HADHB, trifunctional enzyme subunit β; IDH2, isocitrate dehydrogenase; IDH3B, isocitrate dehydrogenase 3β; IDH3G, isocitrate dehydrogenase, subunit γ; OGDH, 2-oxoglutarate dehydrogenase; PC, pyruvate carboxylase; PDHX, pyruvate dehydrogenase protein X component; SLC25A20, mitochondrial carnitine/acylcarnitine carrier protein; TIMM44, translocase of inner mitochondrial membrane 44 homolog; TIMM50, translocase of inner mitochondrial membrane 50 homolog; UCP1, uncoupling protein 1.

changes in mitochondrial proteins in response to hibernation for a better understanding of the molecular mechanisms underlying functional adaptations in BAT mitochondria. Our results suggest that the regulation of BAT function is not entirely at the mitochondrial level because BAT mitochondria are primed to produce heat regardless of the season.

Perspectives and Significance

Brown adipose tissue mitochondria play an important role in the adaptive thermogenesis portrayed by the thirteen-lined ground squirrel. Results from this study further validate the importance that BAT mitochondria play during hibernation, as mitochondrial proteins for fatty acid handling and metabolism are enhanced during hibernation (Fig. 6). In addition, functional analysis on mitochondrial bioenergetics also show increased respiratory capacity of BAT mitochondria during hibernation, all of which contributes to the massive amount of heat generated by BAT for arousals (Fig. 6).

This study improves our understanding of the metabolic feats in a hibernator. Future studies should consist of identifying and characterizing novel protein isoforms, such as alternative splice variants, single amino acids variants, mutations, and post-translational modifications of mitochondrial proteins. Careful analysis of these amino acid variants may provide essential underpinnings into the hibernation phenotype and aid in better understanding of how BAT function is maintained throughout hibernation. Additionally, future functional studies involving various fuels, such as fatty acid derivatives, should be conducted to investigate whether specific substrates at different temperatures play a role in the overall thermogenic capacity of BAT mitochondria across the year. Even assessing coupled BAT mitochondria may provide mechanistic insight of BAT and aid in understanding the overall mitochondrial metabolism of a natural hibernator.

ACKNOWLEDGMENTS

We are very appreciative of the University of Minnesota Center for Mass Spectrometry and Proteomics. Specifically, we sincerely thank Katie Vermillion, Todd Markowski, LeAnn Higgins, Pratik Jagtap, and Tim Griffin for their patience, guidance, technical assistance, and resources associated with BAT mitoproteomics. We also thank Charlie Sieberg and Alex Theis for their

assistance with measuring mitochondrial respiration rates. Lastly, we thank Clay Carter for use of his sonicator.

GRANTS

This work was supported by the University of Minnesota McKnight Presidential Endowment Fund and U.S. Army Medical Research and Materiel Command contract number W81XWH-11-0409 to MTA, and NSF grant 114707 to the University of Minnesota Center for Mass Spectrometry and Proteomics.

DISCLOSURES

No conflicts of interest, financial or otherwise, are declared by the authors.

AUTHOR CONTRIBUTIONS

M.A.B., J.A.B., and M.T.A. conception and design of research; M.A.B., C.H., M.W.N., and J.A.B. performed experiments; M.A.B., C.H., M.W.N., and J.A.B. analyzed data; M.A.B., C.H., M.W.N., J.A.B., and M.T.A. interpreted results of experiments; M.A.B. prepared figures; M.A.B. drafted manuscript; M.A.B., C.H., M.W.N., J.A.B., and M.T.A. edited and revised manuscript; M.A.B. and M.T.A. approved final version of manuscript.

REFERENCES

1. **Anderson KJ, Vermillion KL, Jagtap P, Johnson JE, Griffin TJ, Andrews MT.** Proteogenomic analysis of a hibernating mammal indicates contribution of skeletal muscle physiology to the hibernation phenotype. *J Proteome Res* 15: 1253–1261, 2016.
2. **Andrews MT.** Advances in molecular biology of hibernation in mammals. *Bioessays* 29: 431–440, 2007.
3. **Armstrong C, Staples JF.** The role of succinate dehydrogenase and oxaloacetate in metabolic suppression during hibernation and arousal. *J Comp Physiol B* 180: 775–783, 2010.
4. **Brown JCL, Chung DJ, Cooper AN, Staples JF.** Regulation of succinate-fuelled mitochondrial respiration in liver and skeletal muscle of hibernating thirteen-lined ground squirrels. *J Exp Biol* 216: 1736–1743, 2013.
5. **Brown JCL, Gerson AR, Staples JF.** Mitochondrial metabolism during daily torpor in the dwarf Siberian hamster: role of active regulated changes and passive thermal effects. *Am J Physiol Regul Integr Comp Physiol* 293: R1833–R1845, 2007.
6. **Burlington RF, Therriault DG, Hubbard RW.** Lipid changes in isolated brown fat cells from hibernating and aroused thirteen-lined ground squirrels (*Citellus tridecemlineatus*). *Comp Biochem Physiol* 29: 431–437, 1969.
7. **Cannon B, Nedergaard J.** Brown adipose tissue: function and physiological significance. *Physiol Rev* 84: 277–359, 2004.
8. **Cannon B, Nedergaard J.** Studies of thermogenesis and mitochondrial function in adipose tissues. *Methods Mol Biol* 456: 109–121, 2008.
9. **Cannon B.** The mitochondrial ATPase of brown adipose tissue. Purification and comparison with the mitochondrial ATPase from beef heart. *FEBS Lett* 76: 284–289, 1977.
10. **Carey HV, Andrews MT, Martin SL.** Mammalian hibernation: cellular and molecular responses to depressed metabolism and low temperature. *Physiol Rev* 83: 1153–1181, 2003.
11. **Chaffee RRJ, Pengelley ET, Allen JR, Smith RE.** Biochemistry of brown fat and liver of hibernating golden mantled ground squirrels (*Citellus lateralis*). *Can J Physiol Pharmacol* 44: 217–223, 1966.
12. **Chaffee RRJ, Allen JR, Cassuto Y, Smith RE.** Biochemistry of brown fat and liver of cold-acclimated hamsters. *Am J Physiol* 207: 1211–1214, 1964.
13. **Chance B, Williams GR.** Respiratory enzymes in oxidative phosphorylation: III. The steady state. *J Biol Chem* 217: 409–427, 1955.
14. **Chung D, Lloyd GP, Thomas RH, Guglielmo CG, Staples JF.** Mitochondrial respiration and succinate dehydrogenase are suppressed early during entrance into a hibernation bout, but membrane remodeling is only transient. *J Comp Physiol B* 181: 699–711, 2011.

14a. **De Sousa Abreu R, Penalva LO, Marcotte EM, Vogel C.** Global signatures of protein and mRNA expression levels. *Mol Biosyst* 5: 1512–1526, 2009.

15. **Eddy SF, Storey KB.** Up-regulation of fatty acid-binding proteins during hibernation in the little brown bat, *Myotis lucifugus*. *Biochim Biophys Acta* 1676: 63–70, 2004.
16. **Fedotcheva NJ, Sharyshev AA, Mironova GD, Kondrashova MN.** Inhibition of succinate oxidation and K^+ transport in mitochondria during hibernation. *Comp Biochem Physiol* 82: 191–195, 1985.
17. **Foss EJ, Radulovic D, Shaffer SA, Goodlett DR, Kruglyak L, Bedalov A.** Genetic variation shapes protein networks mainly through non-transcriptional mechanisms. *PLoS Biol* 9: e1001144, 2011.
18. **Geiser F.** Reduction of metabolism during hibernation and daily torpor in mammals and birds: temperature effect or physiological inhibition? *J Comp Physiol B* 158: 25–37, 1988.
19. **Gomes LC, Di Benedetto G, Scorrano L.** During autophagy mitochondria elongate, are spared from degradation and sustain cell viability. *Nat Cell Biol* 13: 589–598, 2011.
20. **Grabek KR, Martin SL, Hindle AG.** Proteomics approaches shed new light on hibernation physiology. *J Comp Physiol B* 185: 607–627, 2015.
21. **Gry M, Rimini R, Strömberg S, Asplund A, Pontén F, Uhlén M, Nilsson P.** Correlations between RNA and protein expression profiles in 23 human cell lines. *BMC Genomics* 10: 365, 2009.
22. **Guppy M, Withers P.** Metabolic depression in animals: physiological perspectives and biochemical generalizations. *Biol Rev* 74: 1–40, 1999.
23. **Hampton M, Melvin RG, Andrews MT.** Transcriptomic analysis of brown adipose tissue across the physiological extremes of natural hibernation. *PLoS One* 8: e85157, 2013.
24. **Hampton M, Melvin RG, Kendall AH, Kirkpatrick BR, Peterson N, Andrews MT.** Deep sequencing the transcriptome reveals seasonal adaptive mechanisms in a hibernating mammal. *PLoS One* 6: e27021, 2011.
25. **Hampton M, Nelson BT, Andrews MT.** Circulation and metabolic rates in a natural hibernator: an integrative physiological model. *Am J Physiol Regul Integr Comp Physiol* 299: R1478–R1488, 2010.
26. **Hindle AG, Martin SL.** Intrinsic circannual regulation of brown adipose tissue form and function in tune with hibernation. *Am J Physiol Endocrinol Metab* 306: E284–E299, 2014.
27. **Hook E, Guzman ES.** The respiration of brown adipose tissue and kidney of the hibernating and non-hibernating ground squirrel. *Am J Physiol* 133: 56–63, 1941.
28. **Houste̊k J, Cannon B, Lindberg O.** Gylcerol-3-phosphate shuttle and its function in intermediary metabolism of hamster brown-adipose tissue. *Eur J Biochem* 54: 11–18, 1975.
29. **Huang DAW, Sherman BT, Lempicki RA.** Systematic and integrative analysis of large gene lists using DAVID bioinformatics resources. *Nat Protoc* 4: 44–57, 2009.
30. **Huang DAW, Sherman BT, Lempicki RA.** Bioinformatics enrichment tools: paths toward the comprehensive functional analysis of large gene lists. *Nucleic Acids Res* 37: 1–13, 2009.
31. **Huang DW, Sherman BT, Tan Q, Collins JR, Alvord WG, Roayaei J, Stephens R, Baseler MW, Lane HC, Lempicki RA.** The DAVID gene functional classification tool: a novel biological module-centric algorithm to functionally analyze large gene lists. *Genome Biol* 8: R183, 2007.
32. **Kelly DP, Scarpulla RC.** Transcriptional regulatory circuits controlling mitochondrial biogenesis and function. *Genes Dev* 18: 357–368, 2004.
33. **Li L, Pan R, Li R, Niemann B, Aurich AC, Chen Y, Rohrbach S.** Mitochondrial biogenesis and peroxisome proliferator-activated receptor-γ coactivator-1α (PGC-1α) deacetylation by physical activity: intact adipocytokine signaling is required. *Diabetes* 60: 157–167, 2011.
34. **Li Z, Graham BH.** Measurement of mitochondrial oxygen consumption using a Clark electrode. *Methods Mol Biol* 837: 63–72, 2012.
35. **Liesa M, Shirihai OS.** Mitochondrial dynamics in the regulation of nutrient utilization and energy expenditure. *Cell Metab* 17: 491–506, 2013.
36. **Lotz C, Lin AJ, Black CM, Zhang J, Lau E, Deng N, Wang Y, Zong NC, Choi JH, Xu T, Liem DA, Korge P, Weiss JN, Hermjakob H, Yates JR, Apweiler R, Ping P.** Characterization, design, and function of the mitochondrial proteome: from organs to organisms. *J Proteome Res* 13: 433–446, 2014.
37. **Lutfalla G, Uze G.** Performing quantitative reverse-transcribed polymerase chain reaction experiments. *Methods Enzymol* 410: 386–400, 2006.
38. **Malatesta M, Battistelli S, Rocchi MB, Zancanaro C, Fakan S, Gazzanelli G.** Fine structural modifications of liver, pancreas and brown adipose tissue mitochondria from hibernating, arousing and euthermic dormice. *Cell Biol Int* 25: 131–138, 2001.
39. **Malik AN, Shahni R, Rodriguez-de-Ledesma A, Laftah A, Cunningham P.** Mitochondrial DNA as a non-invasive biomarker: accurate quantification using real time quantitative PCR without co-amplification of pseudogenes and dilution bias. *Biochem Biophys Res Commun* 412: 1–7, 2011.

40. **McKee G, Andrews JF.** Brown adipose tissue lipid is the main source of energy during arousal of the golden hamster (*Mesocricetus auratus*). *Comp Biochem Physiol A* 96: 485–488, 1990.
41. **Lin-Moshier Y, Sebastian PJ, Higgins L, Sampson ND, Hewitt JE, Marchant JS.** Re-evaluation of the role of calcium homeostasis endoplasmic reticulum protein (CHERP) in cellular calcium signaling. *J Biol Chem* 288: 355–367, 2013.
42. **Mráček T, Drahota Z, Houštěk J.** The function and the role of the mitochondrial glycerol-3-phosphate dehydrogenase in mammalian tissues. *Biochim Biophys Acta* 1827: 401–410, 2013.
43. **Nedergaard J, Cannon B.** Preferential utilization of brown adipose tissue lipids during arousal from hibernation in hamsters. *Am J Physiol Regul Integr Comp Physiol* 247: R506–R512, 1984.
44. **Nicholls DG, Locke RM.** Thermogenic mechanisms in brown fat. *Physiol Rev* 64: 1–64, 1984.
45. **Nie L, Wu G, Culley DE, Scholten JC, Zhang W.** Integrative analysis of transcriptomic and proteomic data: challenges, solutions and applications. *Crit Rev Biotechnol* 27: 63–75, 2007.
46. **Ohkawa KI, Vogt MT, Farber E.** Unusually high mitochondrial alpha glycerophosphate dehydrogenase activity in rat brown adipose tissue. *J Cell Biol* 41: 441–449, 1969.
47. **Pascal LE, True LD, Campbell DS, Deutsch EW, Risk M, Coleman IM, Eichner LJ, Nelson PS, Liu AY.** Correlation of mRNA and protein levels: cell type-specific gene expression of cluster designation antigens in the prostate. *BMC Genomics* 9: 246, 2008.
48. **Rasband WS.** ImageJ. http://imagej nih.gov/ij/, 1997.
49. **Russeth KP, Higgins L, Andrews MT.** Identification of proteins from non-model organisms using mass spectrometry: application to a hibernating mammal. *J Proteome Res* 5: 829–839, 2006.
50. **Schwartz C, Hampton M, Andrews MT.** Seasonal and regional differences in gene expression in the brain of a hibernating mammal. *PLoS One* 8: e58427, 2013.
51. **Schwartz C, Hampton M, Andrews MT.** Hypothalamic gene expression underlying pre-hibernation satiety. *Genes Brain Behav* 14: 310–318, 2015.
52. **Silva AM, Oliveira PJ.** Evaluation of respiration with clark type electrode in isolated mitochondria and permeabilized animal cells. *Methods Mol Biol* 810: 7–24, 2012.
53. **Snapp BD, Heller HC.** Suppression of metabolism during hibernation in ground squirrels (*Citellus lateralis*). *Physiol Zool* 54: 297–307, 1981.
55. **Staples JF, Brown JCL.** Mitochondrial metabolism in hibernation and daily torpor: a review. *J Comp Physiol B* 178: 811–827, 2008.
56. **Staples JF.** Metabolic suppression in mammalian hibernation: the role of mitochondria. *J Exp Biol* 217: 2032–2036, 2014.
57. **Storey KB, Storey JM.** Metabolic rate depression and biochemical adaptation in anaerobiosis, hibernation and estivation. *Q Rev Biol* 65: 145–174, 1990.
58. **Vermillion KL, Jagtap P, Johnson JE, Griffin TJ, Andrews MT.** Characterizing cardiac molecular mechanisms of mammalian hibernation via quantitative proteogenomics. *J Proteome Res* 14: 4792–4804, 2015.
59. **Yang F, Shen Y, Camp DG, Smith RD.** High-pH reversed-phase chromatography with fraction concatenation for 2D proteomic analysis. *Expert Rev Proteomics* 9: 129–134, 2012.
60. **Yin S, Xue J, Sun H, Wen B, Wang Q, Perkins G, Zhao HW, Ellisman MH, Hsiao YH, Yin L, Xie Y, Hou G, Zi J, Lin L, Haddad GG, Zhou D, Liu S.** Quantitative evaluation of the mitochondrial proteomes of *Drosophila melanogaster* adapted to extreme oxygen conditions. *PLoS One* 8: e74011, 2013.
61. **Youle RJ, van der Bliek AM.** Mitochondrial fission, fusion, and stress. *Science* 337: 1062–1065, 2012.
62. **Zhang J, Nuebel E, Wisidagama DR, Setoguchi K, Hong JS, Van Horn CM, Imam SS, Vergnes L, Malone CS, Koehler CM, Teitell MA.** Measuring energy metabolism in cultured cells, including human pluripotent stem cells and differentiated cells. *Nat Protoc* 7: 1068–1085, 2012.